Two-Dimensional Order in β-Sheet Peptide Monolayers

Hanna Rapaport,*,‡ Kristian Kjaer,§ Torben R. Jensen,§ Leslie Leiserowitz,† and David A. Tirrell*,‡

Contribution from the Division of Chemistry and Chemical Engineering, California Institute of Technology, Pasadena, California 91125, Condensed Matter Physics and Chemistry Department, Risø National Laboratory, DK-4000 Roskilde, Denmark, and Department of Materials and Interfaces, Weizmann Institute of Science, Rehovot 76100, Israel

Received June 22, 2000

Abstract: Amphiphilic peptides comprising alternating hydrophilic and hydrophobic amino acid residues were designed to form super-secondary structures composed of self-assembled β-strands as monolayers at the air−water interface. Insights provided by in situ grazing-incidence X-ray diffraction (GIXD), surface pressure vs area isotherms, and Fourier transform infrared spectroscopy allow structural characterization of the assembled nanostructures and rational correlation with the peptide sequence. Peptides seven to seventeen amino acids in length were found to form crystalline arrays with coherence lengths in the range of 100 to 1000 Å. Two-dimensional registry of the self-assembled peptides was induced by placement of proline residues at the peptide termini. The films were found to intercalate ordered arrays of ions between juxtaposed β-sheet ribbons to generate peptide−ion composite phases.

Introduction

The design and assembly of molecular nanostructures of predictable structure and function has become one of the key aims of chemistry and materials science. Progress in the design and characterization of ordered interfaces[1,2] and growing interest in nanometer-scale molecular engineering provide strong incentives to broaden the scope of nanostructured materials and to enhance our understanding of molecular assembly. In the search for advanced materials and new fabrication strategies, it is tempting to try to exploit the intriguing peptide and protein architectures that orchestrate the catalytic and other regulatory tasks in living systems. We and others have demonstrated the use of the secondary structural elements of proteins, i.e. β-strands, helices, and turns, to engineer molecular arrangements amenable to the design of functional nanostructures.[3−5]

Helical macromolecules, including DNA, have been exploited for the formation of ordered assemblies;[5,6] the rigidity of the molecular components generally simplifies the design of supramolecular architectures. In comparison, many peptides and proteins exhibit flexibility that may hamper the formation of ordered assemblies. Indeed, artificial β-sheet proteins which have been shown to form regularly folded crystalline structures in the solid state[4] exhibit only partial order at the air−water interface, with no evidence for regular folding.[7]

In this study our goal is to explore the feasibility of obtaining highly ordered β-strand assemblies at the air−water interface. The crystalline monolayers introduced here represent a new class of ordered assemblies that provide planar scaffolds relevant to a broad spectrum of potential applications in nanometer-scale surface patterning, including catalysis,[8] photoreactive films,[9] optical[10,11] and molecular electronic devices,[12,13] cell guidance substrates,[14] and long-range alignment of nanocrystals.[15−17] A simple and systematic design strategy, coupled with structural characterization involving X-ray diffraction measurements at the air−water interface, provides new insight into the correlation

‡ California Institute of Technology.
§ Risø National Laboratory.
† Weizmann Institute of Science.

(1) Ulman, A. *Self-Assembly of Surfactant Molecules on Solid Surfaces*; Whitesell, K., Ed.; John Wiley and Sons: New York, 1999; pp 1−38.
(2) Rapaport, H.; Kuzmenko, I.; Berfeld, M.; Edgar, R.; Popovits-Biro, R.; Weissbuch, I.; Lahav, M.; Leiserowitz, L. *J. Phys. Chem. B* **2000**, *104*, 1399−1428.
(3) Ghadiri, M. R.; Granaja, J. R.; Milligan, R. A.; Duncan, E. M.; Khazanovich, N. *Nature* **1993**, *355*, 324−327.
(4) Krejchi, M. T.; Atkins, E. D. T.; Waddon, A. J.; Fournier, M. J.; Mason, T. L.; Tirrell, D. A. *Science* **1994**, *265*, 1427−1432.
(5) Yu, S. M.; Conticello, V. P.; Zhang, G.; Kayser, C.; Fournier, M. J.; Mason, T. L.; Tirrell, D. A. *Nature* **1997**, *389*, 167−170.
(6) Winfree, E.; Liu, F. R.; Wenzler, L. A.; Seeman, N. C. *Nature* **1998**, *394*, 539−544.
(7) Self-assembly of the artificial protein $[(AlaGly)_3GluGly]_{36}$ at the air−water interface was examined by in situ GIXD measurements. These studies indicated only weak one-dimensional order arising from the interstrand repeat distance of 4.7 Å, in contrast to highly ordered lamellar crystallites formed by the protein in the solid state. We suggest that the length of the protein and the insufficient difference in hydrophobicity of the repeating constituents amino acids preclude the formation of two-dimensional order at the air−water interface.
(8) Tollner, K.; Popovitz-Biro, R.; Lahav, M.; Milstein, D. *Science* **1997**, *278*, 2100−2102.
(9) Koch, H.; Laschewsky, A.; Ringsdorf, H.; Teng, K. *Makromol. Chem.* **1986**, *187*, 1843−1853.
(10) Berg, R. H.; Hvilsted, S.; Ramanujan, P. S. *Nature* **1996**, *383*, 505−508.
(11) Weissbuch, I.; Bouwman, W. G.; Kjaer, K.; Als-Nielsen, J.; Lahav, M.; Leiserowitz, L. *Chirality* **1998**, *10*, 60−65.
(12) Bumm, L. A.; Arnold, J. J.; Cygan, M. T.; Dunbar, T. D.; Burgin, T. P.; Jones, L., II; Allara, D. L.; Tour, J. M.; Weiss, P. S. *Science* **1996**, *271*, 1705−1707.
(13) Metzger, R. M. *Acc. Chem. Res.* **1999**, *32*, 950−957.
(14) Zhang, S. G.; Yan, L.; Altman, M.; Lassle, M.; Nugent, H.; Frankel, F.; Lauffenburger, D. A.; Whitesides, G. M.; Rich, A. *Biomaterials* **1999**, *20*, 1213−1220.
(15) Fendler, J. H.; Meldrum, F. C. *Adv. Mater.* **1995**, *7*, 607−632.
(16) Shenton, W.; Pum, D.; Sleytr, U. B.; Mann, S. *Nature* **1997**, *389*, 585−587.
(17) Bekele, H.; Fendler, J. H.; Kelly, J. W. *J. Am. Chem. Soc.* **1999**, *121*, 7266−7267.

10.1021/ja002238t CCC: $19.00
Published on Web 11/30/2000

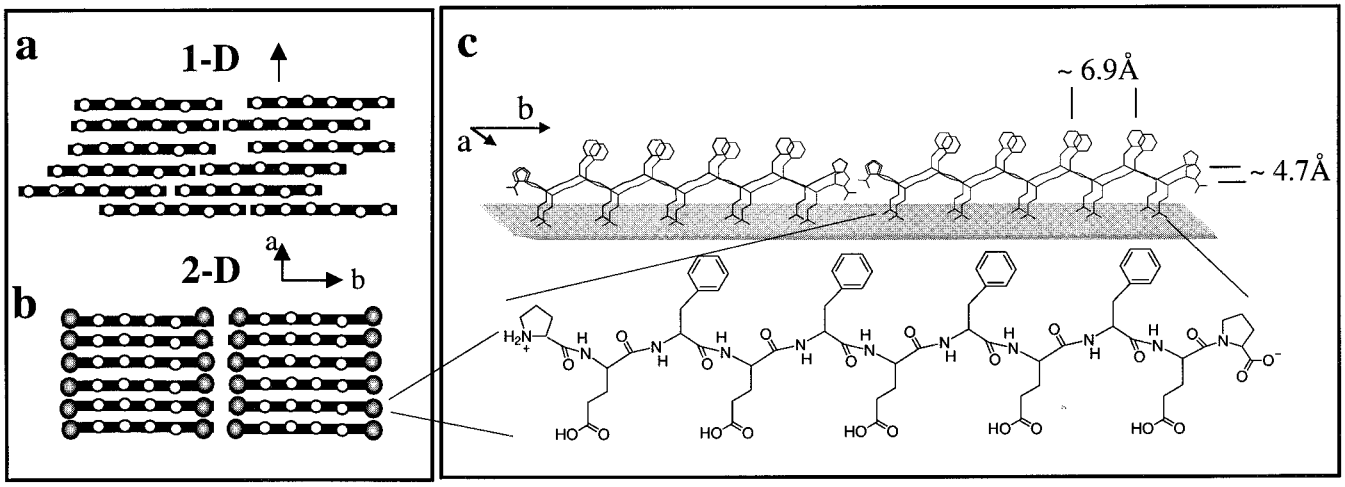

Figure 1. Schematic diagrams of β-strand assemblies at the air−water interface (rods and open dots represent peptide backbones and hydrophobic amino acids, respectively). View down the normal to the β-sheet of (a) one-dimensional order and (b) two-dimensional order induced by distinct chain termini. (c) Schematic representation of the peptide Pro-Glu-(Phe-Glu)$_4$-Pro in the β-pleated conformation and the targeted β-sheet crystalline assembly at the air−water interface. An estimate of the area per molecule can be obtained using the repeat distances of ∼4.7 and ∼6.9 Å that have been observed previously in crystalline β-sheet structures[4] (e.g. 4.7 × 6.9 × 5.5 = 178 Å^2 for the 11 residue peptide).

of peptide sequence and the crystalline properties of peptide monolayers.

Peptides comprising repetitive dyads of hydrophilic and hydrophobic amino acid residues tend to adopt β-pleated sheet arrangements. Local order within monolayers of such peptides at the air−water interface has been inferred from infrared and circular dichroism measurements.[18,19] Spectroscopic data do not, however, provide information on extended order, i.e., order on the nanometer length scale. The flexibility of the peptide backbone and the repetitive nature of the amino acid sequence may induce dislocation defects (Figure 1a) that limit long-range order to one-dimension (1-D), in the direction normal to the peptide backbone. Molecular aggregates with predominantly 1-D order will exhibit absorption spectra typical of β-sheet structures; however, such films do not meet the requirement of 2-D repetitive order that is the goal of this study.

A schematic representation of the 2-D crystalline monolayer targeted in this work is shown in Figure 1b. In such an array of β-sheet peptides the chain termini govern intermolecular interactions between juxtaposed β-sheet ribbons (along *b*), whereas hydrogen bonds along the chain dominate the intermolecular interactions in the direction normal to the peptide chain (along *a*). X-ray diffraction measurements on β-sheet proteins[4] and peptides[20] yield relatively sharp Bragg peaks corresponding to the interstrand (∼4.7−4.8 Å) spacing, indicative of anisotropy in crystalline domain shape that is the result of faster growth along the direction of the interstrand hydrogen bonds (along *a*). We imagined that extended 2-D order in β-strand assemblies might be induced by choosing amino acid termini that would interrupt the network of lateral hydrogen bonds and thereby juxtapose regularly growing peptide ribbons (Figure 1b). This simple approach is evaluated here as a means to eliminate defects and induce extended crystalline packing within the β-sheet film.

The family of peptides examined in this work is represented by the generic sequence X-Y-(Z-Y)$_n$-X, where the N- and C-terminal residues (X) bear charged ammonium and carboxylate groups, respectively, and Y and Z are alternating hydrophilic and hydrophobic amino acids. Variations in amino acid sequence and in the number of dyads (*n*) participating in hydrogen-bond formation are expected to tune the intermolecular interactions and therefore the dimensions of the 2-D ordered β-sheet domains. Proline (Pro), which has been previously shown to be a potent breaker of α-helix and β-sheet structures,[21,22] was chosen as the terminal amino acid (X). Three characteristic features of the Pro residue were expected to facilitate the ordered structure: (i) The tertiary amide at the C-terminus of the peptide, which cannot participate as a donor in the hydrogen bond array, should make dislocation defects energetically unfavorable, (ii) the restricted dihedral angle (ϕ) of Pro (ca. −60°), which is significantly different from that of β-sheet peptides[23] (ϕ ca. −120 to −150°) should make inclusion of Pro in the interior of a β-sheet ribbon sterically unfavorable, and (iii) the geometric constraints imposed by the cyclic Pro side chain should minimize librational motion and dynamic disorder at the ribbon edge. Attractive electrostatic interactions between the chain termini were expected to juxtapose the β-sheet ribbons along the *b* direction (Figure 1b). Glutamic acid (Glu) in its protonated state was selected as the hydrophilic amino acid (Y), to stabilize the assembly by formation of a hydrogen-bond network between carboxyl groups bridging adjacent strands along the *a* direction. Phenylalanine (Phe) was chosen as the hydrophobic amino acid (Z); its relatively large side chain allows the phenyl moiety to span the spacing between neighboring strands in the ensemble, providing favorable side-chain to side-chain interactions.[24,25] The repeat distances (Figure 1c) of ∼4.7 and ∼6.9 Å (along the *a* and *b* directions respectively) have been observed in crystalline β-sheet structures[4,26] and the β-pleated conformation ensures that the area per amino acid side chain, on each face of the sheet (ca. 4.7 × 6.9 = 32.4 Å^2), is decidedly larger than the cross-sectional area of the extended Glu side chain (∼18 Å^2) or the phenyl ring of Phe (∼25 Å^2). The peptides Pro-Glu-(Phe-

(18) Osterman, D.; Mora, R.; Kezdy, F. J.; Kaiser, E. T.; Meredith, S. C. *J. Am. Chem. Soc.* **1984**, *106*, 6845−6847.
(19) DeGrado, W. F.; Lear, J. D. *J. Am. Chem. Soc.* **1985**, *107*, 7684−7689.
(20) Choo, D. W.; Schneider, J. P.; Graciani, N. R.; Kelly, J. W. *Macromolecules* **1996**, *29*, 355−366.
(21) Minor, D. L., Jr.; Kim, P. S. *Nature* **1994**, *367*, 660−663.
(22) Wouters, M. A.; Curmi, P. M. G. *Proteins* **1995**, *22*, 119−131.
(23) Salemme, F. R.; Weatherford, D. W. *J. Mol. Biol.* **1981**, *146*, 119−141.
(24) Hunter, C. A.; Singh, J.; Thornton, J. M. *J. Mol. Biol.* **1991**, *218*, 837−846.
(25) Smith, C. K.; Regan, L. *Science* **1995**, *270*, 980−982.
(26) Krimm, S.; Bandekar, J. *Adv. Protein Chem.* **1986**, *38*, 181−364.

Glu)$_n$-Pro, n = 2, 4, 5, and 7, were prepared by solid-phase organic synthesis and detailed structural characterization is presented here for the undecapeptide Pro-Glu-(Phe-Glu)$_4$-Pro (Figure 1c). The peptides (Phe-Glu)$_5$-Phe and Leu-Cys-(Phe-Ser)$_3$-Phe were also examined to evaluate the structural roles played by the hydrophilic side chains and the terminal amino acid residues.

Experimental Section

Peptides composed of L amino acids were prepared by solid-phase methods using t-Boc chemistry and purified on a reverse-phase XTerra (Waters, MA) HPLC column using a gradient of 0−50% CH_3CN in 0.1 M $(NH_4)HCO_3$. Purity was confirmed by MALDI mass spectrometry.

Monolayers were prepared by spreading a solution of the peptide in trifluoroacetic acid/chloroform (1:9 v/v) at a concentration of approximately 0.1 mg/mL. Surface pressure−area isotherms of the monolayer films were measured using a KSV minitrough (KSV Instruments LTD, Helsinki, Finland). The nominal area per molecule, A, is the area available on the Langmuir trough divided by the number of molecules spread.

FTIR spectra were measured on a Nicolet 860 instrument equipped with a mercury−cadmium−telluride detector at 2 cm^{-1} resolution under a nitrogen atmosphere. A monolayer of Pro-Glu-(Phe-Glu)$_4$-Pro was prepared at the air−water interface (A = 180 Å^2/molecule) and transferred to a 45° ATR ZnSe prism face which was manually lowered in a horizontal orientation until the prism face touched the water surface. The same transfer procedure was repeated for the opposite face of the ZnSe prism. The ATR crystal was mounted on a vertically oriented ATR bench (Wilmad). A total of 1000 scans was averaged for each spectrum.

GIXD experiments were performed with the liquid surface diffractometer at the undulator BW1 beam line at the Hasylab synchrotron source (Hamburg, Germany). The peptide films were spread at room temperature and diffraction measurements were performed at 5 °C. A monochromatic X-ray beam was adjusted to strike the liquid surface at an incident angle ($\alpha \approx 0.85\alpha_c$ where α_c is the critical angle for total external reflection) that maximizes surface sensitivity. The dimensions of the footprint of the incoming X-ray beam on the liquid surface were approximately 2 × 50 mm^2. GIXD signals were obtained from two-dimensional crystallites randomly oriented about the water surface normal. The scattered intensity was collected by means of a position-sensitive detector (PSD) which intercepts photons over the range $0.0 \le q_z \le 0.9$ Å^{-1}, q_z being the out-of -plane component of the scattering vector. Measurements were performed by scanning the horizontal component, $q_{xy} \approx 4\pi \sin\theta_{xy}/\lambda$, of the scattering vector, where $2\theta_{xy}$ is the angle between the incident and diffracted beam projected onto the horizontal plane. The diffraction data are represented in two ways: (1) The GIXD pattern $I(q_{xy})$, obtained by integrating over the whole q_z window of the PSD, shows Bragg peaks. (2) Bragg rod intensity profiles are the scattered intensities $I(q_z)$ recorded in channels along the PSD but integrated across the q_{xy} range of each Bragg peak. The q_{xy} positions of the Bragg peaks yield the lattice repeat distances $d = 2\pi/q_{xy}$, which may be indexed by the two Miller indices h,k to yield the unit cell. The full width at half maximum (fwhm) of the Bragg peaks yields[27] the lateral 2D crystalline coherence length $L_{xy} \approx 0.9(2\pi)/\text{fwhm}(q_{xy})$. The width of the Bragg rod profile along q_z gives a measure of the thickness[28] of the crystalline film $L_z \approx 0.9(2\pi)/\text{fwhm}(q_z)$. The diffraction data are represented either as the measured intensities or after correction for the Lorenz−polarization and active area (LPA) factors. The intensity at a particular value of q_z in a Bragg rod is proportional to the square of the molecular structure factor, $|F_{hk}(q_z)|^2$. Thus Bragg rod intensities for the proposed models can be calculated using the atomic coordinates in the unit cell. The CERIUS^2 computational package (Molecular Simulations Inc., San Diego. CA) was used for the construction of molecular models and minimization of lattice energy.

(27) Guinier, A. *X-ray Diffraction*; Freeman: San Francisco, 1968.

(28) Als-Nielsen, J.; Jacquemain, D.; Kjaer, K.; Leveiller, F.; Lahav, M.; Leiserowitz, L. *Phys. Rep.* **1994**, *246*, 252−313.

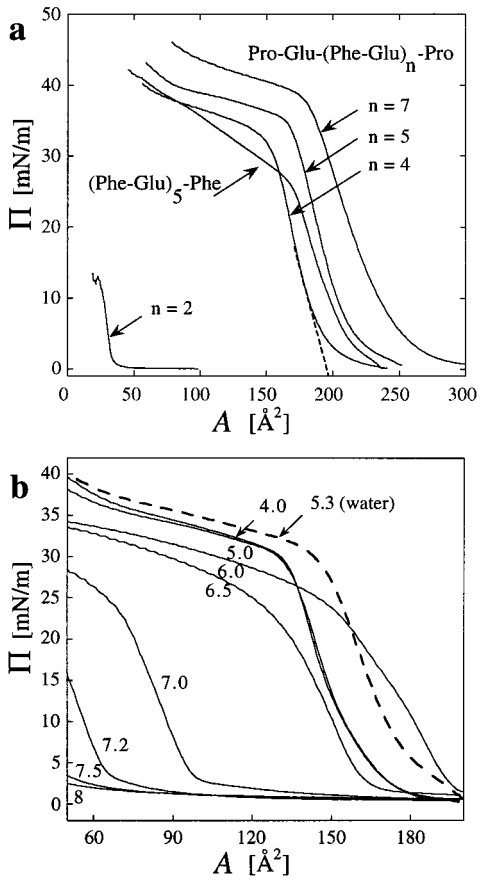

Figure 2. (A) Surface pressure−area (Π−A) isotherms of the peptides Pro-Glu-(Phe-Glu)$_n$-Pro, n = 2,4,5,7, and (Phe-Glu)$_5$-Phe on deionized water at pH 5.3. The limiting molecular areas for Pro-Glu-(Phe-Glu)$_n$-Pro, n = 4, 5, and 7, on deionized water were determined from tangents drawn to the slope of each curve (see dashed line for example for the n = 4 peptide). (B) Π−A isotherms of the peptide Pro-Glu-(Phe-Glu)$_4$-Pro on deionized water (pH 5.3) and on 0.1 M phosphate buffer at various pH values, measured at 20 °C. Films were allowed to equilibrate for 10 min before compression.

Results and Discussion

Surface Pressure Area Isotherms. Surface pressure vs molecular area (Π−A) isotherms of the peptides Pro-Glu-(Phe-Glu)$_n$-Pro (n = 4, 5, and 7) on deionized water at pH 5.3 (Figure 2a) are consistent with the expectation that the peptide chains are oriented with their long molecular axes parallel to the water surface (Figure 2a). The limiting molecular areas for the peptides on deionized water (195, 215, and 255 Å^2, respectively) are in reasonable agreement with the estimated values of the area per molecule (178, 211, and 276 Å^2, respectively) calculated by using the dimensions depicted in Figure 1c. The shortest peptide, Pro-Glu-(Phe-Glu)$_2$-Pro, displays a limiting area per molecule (Figure 2a) of ca. 40 Å^2, much smaller than the expected value of about 115 Å^2, suggesting partial dissolution of the peptide into the subphase. The peptide (Phe-Glu)$_5$-Phe exhibits Π−A behavior slightly different from that of Pro-Glu-(Phe-Glu)$_4$-Pro, with a collapse pressure at ca.25 mN/m (as opposed to ca. 35 mN/m for the latter peptide), pointing to higher rigidity and stronger intermolecular interactions in the Pro-Glu-(Phe-Glu)$_4$-Pro monolayer.

The effect of ionization of the Glu carboxyl moieties on the stability of the film was determined by examining Π−A isotherms for Pro-Glu-(Phe-Glu)$_4$-Pro on 0.1 M potassium phosphate buffers, at pH values ranging from 4 to 8 (Figure 2b). The behavior of the peptide films exhibits a strong

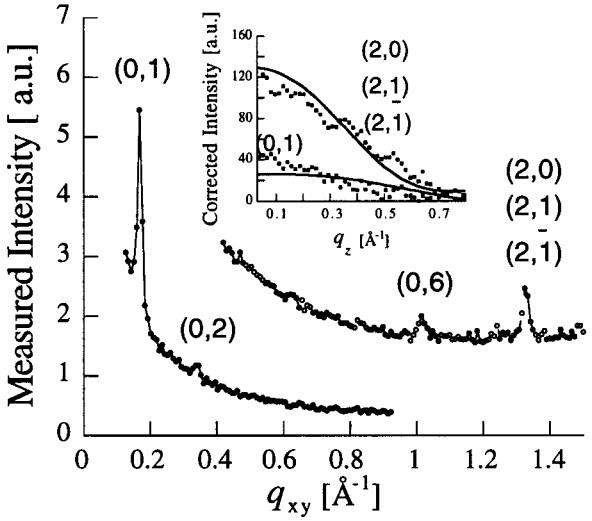

Figure 3. The observed GIXD pattern $I(q_{xy})$ of the crystalline monolayer Pro-Glu-(Phe-Glu)$_4$-Pro film on deionized (pH 5.3) water, uncorrected for Lorenz-polarization and active area (LPA) factors (see Methods). The two sets of data were collected from the same film with different slit settings in the GIXD setup. Inset: The observed Bragg rod intensity profiles $I(q_z)$ of the Bragg peaks at $q_{xy} = 0.166$ and 1.329 Å^{-1} (□) each corrected for LPA factor and X-ray beam damage effects. The calculated Bragg rod profiles (—) correspond to the *APTsp* model (vide infra). In accordance with the *APT* model (vide infra) the peaks at $q_{xy} = 0.166$, 0.332, 1.007 Å^{-1} are indexed (0,1), (0,2), and (0,6), while the peak at 1.329 Å^{-1} is the superposition of (2,0), (−2,1), and (2,1). In a different set of GIXD measurements (not shown), two additional Bragg peaks at $q_{xy} = 0.504$ and 1.616 Å^{-1} were detected that match the *APT* unit cell, and may be indexed (0,3) and (2,6), respectively. The latter confirms the proposed γ angle of the unit cell that is manifested by a 2.4 Å offset between neighboring ribbons. This offset between ribbons leads to a weakening of the calculated intensity of the (2,0) Bragg peak in agreement with the observed data.

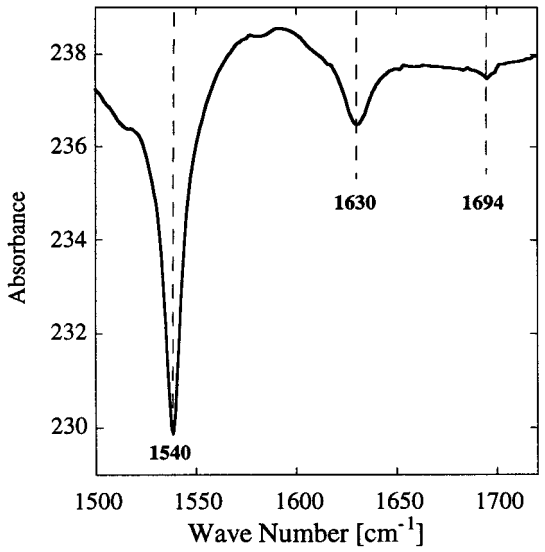

Figure 4. ATR infrared spectrum of Pro-Glu-(Phe-Glu)$_4$-Pro monolayer transferred to a ZnSe prism. The relatively high absorption intensity of the amide II compared to that of amide I may indicate a preferred orientation of the β-sheet domains on the ZnSe crystal surface.

dependence on the pH of the subphase: increasing pH yields smaller limiting areas per molecule and lower surface pressures at fixed values of the molecular area. The apparent dissolution of the film into the subphase at elevated pH values can be attributed to an increase in charge density as a result of Glu carboxyl deprotonation. The pK_a of the Glu side-chain carboxyl group[29] is typically ca. 4.5, yet the $\Pi-A$ isotherms (Figure 2b) suggest that at pH ∼5.3 the Glu residues at the interface are predominantly protonated. A positive shift in pK_a of the carboxyl groups of Glu-rich polypeptides[30] has been observed previously and has been attributed to charge−charge repulsion or to hydrophobic hydration effects. Similar effects may contribute to the pH-dependent behavior of the Pro-Glu-(Phe-Glu)$_4$-Pro monolayer. The deprotonation of carboxyl groups in films at hydrophobic−hydrophilic interfaces has also been observed to shift to higher pH values.[31−33] This behavior is attributed to an interfacial electrical potential[31] that induces elevated proton concentrations at such interfaces.

Grazing-Incidence X-ray Diffraction. Grazing-incidence X-ray diffraction (GIXD) experiments on Pro-Glu-(Phe-Glu)$_4$-Pro monolayer films on water (pH 5.3) provide clear evidence for assembly of the peptide into crystalline β-sheet monolayers. Diffraction peaks are obtained even at low surface pressure and large nominal surface area per molecule (270 Å^2), demonstrating strong interactions between peptide chains that lead to formation of two-dimensional crystals. The GIXD pattern (Figure 3) exhibits four distinct Bragg peaks at $q_{xy} = 0.166$, 0.332, 1.007, and 1.329 Å^{-1}, which can be indexed on the basis of the structural model shown schematically in Figure 1c. The Bragg peak at $q_{xy} = 1.329$ Å^{-1} corresponds to a spacing of 4.7 Å, which is characteristic of crystalline β-sheet systems. The 4.7 Å spacing is generated by pleated peptide strands interlinked by N−H···O═C hydrogen bonds, and constitutes strong evidence for formation of extended hydrogen-bonded ribbons. The Bragg peaks at $q_{xy} = 0.166$, 0.332, and 1.007 Å^{-1} correspond to the first-, second-, and sixth-order reflections of a 37.4 Å spacing. We attribute this spacing to the repeat distance defined by juxtaposition of neighboring hydrogen-bonded ribbons (vide infra). The full widths at half-maxima, fwhm(q_z), of the Bragg rods (Figure 3 inset) along q_z indicate a crystalline film ∼8 Å thick, implying that not only the peptide backbone but also the amino acid side chains are ordered within the crystalline monolayer. The crystalline coherence length L, a measure of the extent of lateral molecular order, as estimated from fwhm(q_{xy}) of the Bragg peaks, is approximately 400 Å along both the 4.7 Å and the 37.4 Å spacing directions.

Structural Models. Given that in the monolayer crystal the peptide backbone assumes the β-strand conformation as established by the observed 4.7 and 37.4 Å spacings, adjacent peptide chains may be arranged in either a parallel or an antiparallel mode. The antiparallel arrangement should in principle give rise to a Bragg reflection at a spacing of 2 × 4.7 Å, which is not observed. Nonetheless, the absence of this peak does not preclude the antiparallel molecular packing motif. This reflection is expected to be weak due to the similarity in the backbone structure of the peptide strands separated by the 4.7 Å spacing. In our preliminary structural modeling, three types of structures (denoted *AP*, *P*, and *APT* respectively) have been examined. In the *AP* model, the unit cell ($a = 9.5$ Å, $b = 37.5$ Å, $\gamma = 93.7°$) contains two molecules related by crystallographic 2-fold symmetry, generating the antiparallel β-sheet hydrogen bond motif that associates the peptides along the 4.7 Å spacing. The

(29) Tanford, C.; Kirkwood, J. G. *J. Am. Chem. Soc.* **1957**, *79*, 5333−5339.
(30) Urry, D. W.; Peng, S. Q.; Parker, T. M.; Gowda, D. C.; Harris, R. D. *Angew. Chem., Int. Ed. Engl.* **1993**, *32*, 1440−1442.
(31) Davies, J. T.; Rideal, E. K. *Interfacial Phenomena*; Academic Press: New York, 1961.
(32) Miranda, B. P.; Du, Q.; Shen, Y. R. *Chem. Phys. Lett.* **1998**, *286*, 1−8.
(33) Chen, H.; Hsu, S. L.; Tirrell, D. A.; Stidham, H. D. *Langmuir* **1997**, *13*, 4774−4778.

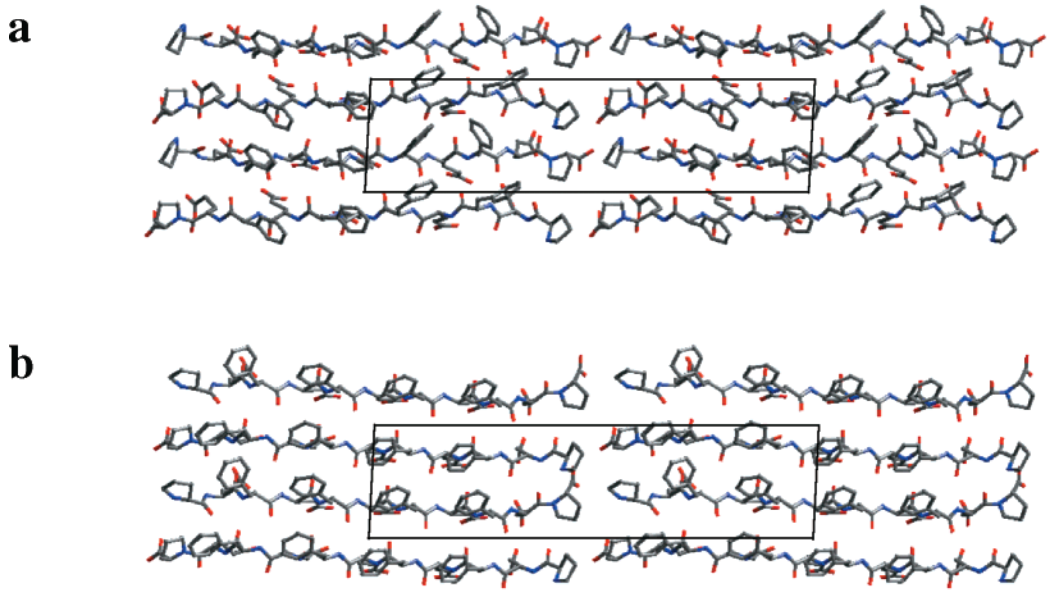

Figure 5. (a,b) The two unit cell structures *APT+b* and *APT-b* whose superposition yields a calculated diffraction pattern that fits the observed GIXD data.

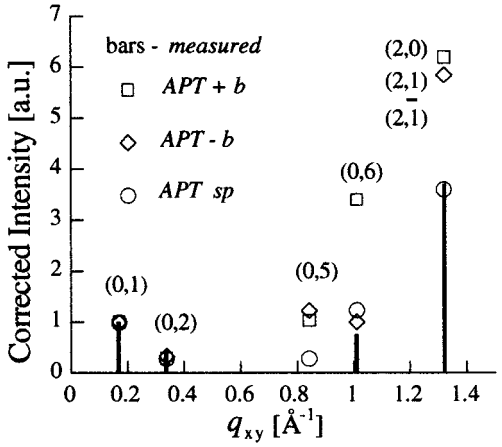

Figure 6. Measured and calculated Bragg peak intensities, $I(q_{xy})$, integrated along the scattering vector components q_{xy} and q_z normalized to the (0,1) intensity. The measured intensities (bars) were corrected for LPA and beam damage effects. Calculated intensities shown for three model structures, *APT+b* (□), *APT-b* (◇), and for *APTsp* that denotes the calculated diffraction pattern of the *APT+b* and *APT-b* superposition model (○).

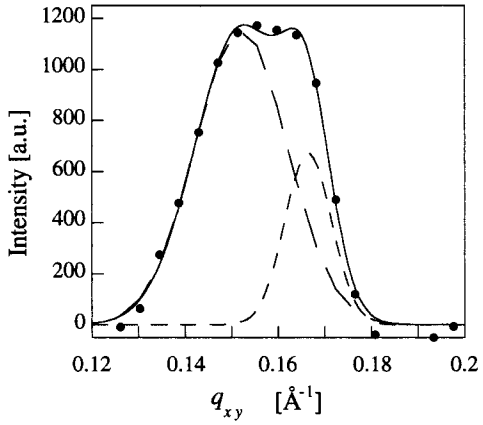

Figure 7. Part of the GIXD pattern $I(q_{xy})$ Pro-Glu-(Phe-Glu)$_4$-Pro monolayer on 0.1 M RbCl, showing the split Bragg peak (dots = observed data) arising from a contribution of two phases, with lattice spacings of 41.5 Å, $q_{xy} = 0.151$ Å^{-1} (−), and 37.7 Å, $q_{xy} = 0.166$ Å^{-1} (- - -), as determined by a two-peak Gaussian fit to the observed data (full line). Higher order (0,*h*) Bragg peaks were not detected for the peptide-RbCl phase.

assigned γ angle (Figure 3, legend) introduces a 9.5/4 = 2.4 Å offset between juxtaposed ribbons in the lattice. The *APT* model, with the same unit cell dimensions, has the peptide backbones related by pseudo-2-fold symmetry, yielding an antiparallel β-sheet structure but with amino acid side chains that are relaxed to assume any energetically favorable conformation. The *P* structure has one molecule per unit cell (a = 9.5/2 Å and the remaining dimensions are identical to that of the *AP* model), generating a parallel β-sheet.

Principal molecular packing features of the monolayer of Pro-Glu-(Phe-Glu)$_4$-Pro could be extracted by X-ray structure factor calculations of molecular models that were refined to provide a good fit to the observed GIXD pattern. Lattice energy minimization calculations (Cerius^2) were also applied to improve intermolecular and particularly side-chain interactions of the proposed models. The best *AP* model that has been generated (but which does not yield a satisfactory fit to the observed X-ray data) has Phe side chains along the 4.7 Å spacing pointing their phenyl rings in opposite directions, precluding favorable side chain intermolecular contacts. The *P* model, with Phe side chains related by pseudotranslation along the peptide backbone, provides an arrangement that may lead to attractive phenyl−phenyl interactions across the 4.7 Å spacing,[24] and results in an improved fit between calculated and observed diffraction patterns. In the *APT* model also, Phe side chains can pack by pseudotranslation, resulting in a diffraction pattern very similar to that of the *P* model.

Fourier transform attenuated total reflectance (FT-ATR) infrared spectroscopy was used to distinguish between the *P* and *APT* structures.[19] The FT-ATR spectrum of a Pro-Glu-(Phe-Glu)$_4$-Pro monolayer transferred from the air−water interface to a ZnSe crystal displays amide I absorption bands at 1630 and 1694 cm^{-1} and an amide II band at 1540 cm^{-1} (Figure 4) characteristic of the antiparallel β-sheet structure. In particular, the weak 1694 cm^{-1} band constitutes strong evidence for the antiparallel structure, as it has been detected for crystals with the antiparallel β-sheet motif but not for the parallel arrangement.[26,34,35]

Table 1. Crystallographic Data[a] on β-Sheet Nanostructures

	d_b	d_{rb}	L_b	n_b	d_a	L_a	n_a	L_a/L_b	n_a/n_b
Pro-Glu-(Phe-Glu)$_2$-Pro	25.8	3.7	670	26	4.73	930	197	1.4	7.6
Pro-Glu-(Phe-Glu)$_4$-Pro	37.4	3.4	460	12	4.74	430	91	0.9	7.6
Pro-Glu-(Phe-Glu)$_5$-Pro	37.4	2.9	200	5	4.78	90	19	0.45	3.8
Pro-Glu-(Phe-Glu)$_7$-Pro	41.1	2.4	230	6	4.80	90	19	0.4	3.2
(Phe-Glu)$_5$-Phe	very weak				4.68	280	60		
					4.88	380	78		
Leu-Cys-(Phe-Ser)$_3$-Phe	not detected					very weak			

[a] The *b* and *a* subscripts denote the (0,1) and (2,0) crystalline axial directions, respectively, d_b and d_a the corresponding lattice spacings (Å), and d_{rb} the spacing per residue along the *b* axis. *L* is the crystalline coherence length (Å), and n_a and n_b the corresponding numbers of lattice repeats. For (Phe-Glu)$_5$-Phe the observed Bragg peak is split into (2,−1) (upper) and (2,1) (lower) data.

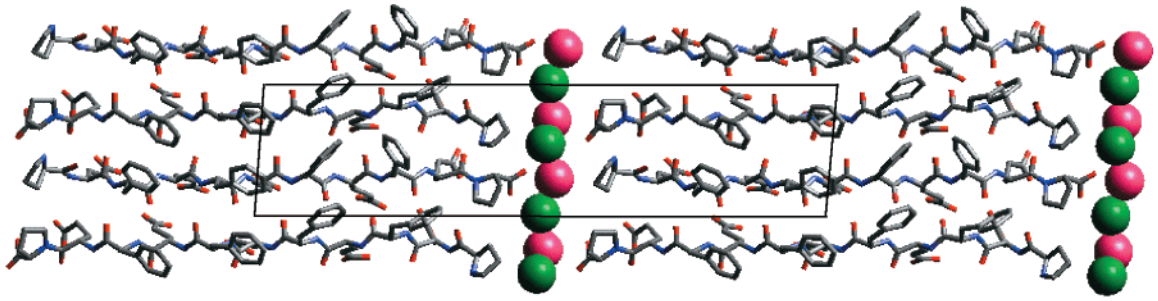

Figure 8. View perpendicular to the air−water interface of the proposed crystal structure of the salt−peptide composite phase, Pro-Glu-(Phe-Glu)$_4$-Pro:RbCl as included within the *APT+b* model. The positions of the Rb and Cl ions (shown in pink and green, respectively) were calculated with energy minimization modules of Cerius[2] after assigning the model the experimentally observed spacing of 41.5 Å.

Model Refinement. The FT-ATR and GIXD results prompted us to focus on refinement of the *APT* model to gain additional insight into the structural characteristics of the two-dimensional lattice. The intramolecular spacing between adjacent amino acids of the same type (Figure 1) gives rise to relatively high librational motions of the side chains and thus to the possibility of various conformations, as supported by energy minimization procedures. Phe side chains along the peptide backbone may assume different orientations in which the central axis of the phenyl rings swivels off the direction of the peptide backbone. The Glu side chains are nearly extended, as supported by structure factor calculations and by energy minimization. Disorder in the side chain conformation may in turn affect the overall orientation of the peptide backbones. Calculated diffraction patterns of various trial models consistently yielded intensities of a few high-order Bragg peaks (such as the (0,5)) which were unacceptably high. Modifications to the model were then made by introducing partial disorder into the crystalline film. The GIXD data could be matched by a model that involves superposition of two structures, designated *APT+b* and *APT-b* (Figures 5 and 6), exhibiting Phe side chains oriented generally in opposite directions relative to the *b* axis. The superposition (*APTsp*) model invokes disorder of the Phe and Glu side chains, namely the random occurrence of the *APT+b* and *APT-b* motifs inside each 2D-crystalline domain. This disorder leads to relatively weak high-order Bragg peaks and also specifically suppresses the (0,5) reflection, in agreement with the observed data (Figure 6). The *APTsp* model implies multiple conformations of the amino acid side chains within the β-sheet assembly, and it is reasonable to assume the existence of other molecular arrangements similar to *APT+b* and *APT-b* within the crystalline film.

Monolayers Spread on Aqueous Salt Solution. The diffraction pattern obtained from Pro-Glu-(Phe-Glu)$_4$-Pro on 0.1 M RbCl resembles that obtained for the same peptide on water, with one significant difference: the Bragg reflection corresponding to the inter-ribbon spacing (0,1) is split, comprising two peaks at $q_{xy} = 0.1510$ and 0.1667 Å^{-1} (Figure 7) that correspond to 41.5 and 37.7 Å spacings, respectively. The 37.7 Å repeat distance is similar to that observed for the Pro-Glu-(Phe-Glu)$_4$-Pro monolayer on water, indicating the existence of a crystalline structure similar to that formed on water. The 41.5 Å spacing may be attributed to a peptide−salt crystalline phase, consisting of hydrogen-bonded peptide ribbons separated by RbCl ions intercalated between the end groups of the peptides (Figure 8). Similar crystalline films of composite peptide−salt structures are formed by Pro-Glu-(Phe-Glu)$_2$-Pro on 0.1 M RbCl, by Pro-Glu-(Phe-Glu)$_5$-Pro on 0.1 M NaCl solution, and by Pro-Glu-(Phe-Glu)$_5$-Pro on 0.1 M $MgCl_2$, demonstrating that ordered β-sheets may intercalate different types of ions.

Variation in Molecular Structure. GIXD studies of (Phe-Glu)$_5$-Phe and Pro-Glu-(Phe-Glu)$_n$-Pro ($n = 2$, 5, and 7) on the surface of pure water exhibit diffraction patterns corresponding to monolayer of peptides lying with their long molecular axes parallel to the air−water interface. The structural data (Table 1) illustrate the correlation between the spatial characteristics of the ordered nanostructure domains and the details of the peptide sequence. Among the peptides studied, the largest crystalline domains are obtained for the shortest chain (Pro-Glu-(Phe-Glu)$_2$-Pro), despite partial dissolution of the peptide in the subphase as inferred from the surface pressure−area isotherm (Figure 2b). The peptide Pro-Glu-(Phe-Glu)$_4$-Pro forms crystalline domains almost isotropic in shape ($L_a/L_b = 0.9$, Table 1) and smaller than those formed by Pro-Glu-(Phe-Glu)$_2$-Pro. However, Pro-Glu-(Phe-Glu)$_4$-Pro displays the strongest Bragg peak intensities, reflecting both its insolubility in water and its strong tendency to organize in the form of a crystalline β-sheet monolayer. The decrease in crystalline coherence lengths along the (0,1) and the (2,0) directions continues also for the longer peptides ($n = 5$ and 7) in the Pro-Glu-(Phe-Glu)$_n$-Pro series. This result may arise from defects of the type shown in Figure 1a or from conformational flexibility that reduces the ability of the longer chains to bind correctly to the growing ends of the

(34) Miyazawa, T.; Blout, E. R. *J. Am. Chem. Soc.* **1961**, *83*, 712−719.
(35) Kim, H. S.; Hartgernik, J. D.; Ghadiri, M. R. *J. Am. Chem. Soc.* **1998**, *120*, 4417−4424.

crystalline arrays. It is noteworthy that the spacing per residue along the (0,1) direction also becomes smaller with increasing chain length for the longer peptides. It is possible that a herringbone motif relating neighboring hydrogen-bonded ribbons along the *b* axis may impose angles other than 90° between the peptide chain axis and the hydrogen-bonding axis, resulting in smaller (0,1) spacings.

Peptides $(Phe\text{-}Glu)_5$-Phe and Pro-Glu-$(Phe\text{-}Glu)_4$-Pro would be expected to yield similar diffraction patterns if they adopt similar packing arrangements. In fact $(Phe\text{-}Glu)_5$-Phe exhibits a very weak (0,1) Bragg peak (Table 1), in contrast to the strong (0,1) intensity observed for Pro-Glu-$(Phe\text{-}Glu)_4$-Pro (cf. Figure 3). Structure factor calculations for $(Phe\text{-}Glu)_5$-Phe show that offsets in peptide registry along the *b* axis (Figure 1a), in steps of ca. 6.8 Å (the intramolecular repeat distance between amino acids of the same type), strongly diminish the intensity of the (0,1) reflection relative to that of the (2,0). Because the terminal residues have no distinct energetic or steric preference for the rim of a growing ribbon, we attribute the weakening of the (0,1) intensity of the $(Phe\text{-}Glu)_5$-Phe monolayer to extensive dislocation defects along the *b* direction of the sort shown schematically in Figure 1a. The peptide Leu-Cys-$(Phe\text{-}Ser)_3$-Phe exhibits another example of 1-D order, as inferred from the single and relatively weak (2,0) Bragg peak which corresponds to the interstrand spacing. These experimental observations support the hypothesis that the two-dimensional crystallinity of β-sheet self-assembled peptides can be rationally controlled through sequence design.

Acknowledgment. We thank Dr. Suzanna Horvath for peptide synthesis, Dr. George Rossman for help in ATR infrared spectroscopy, and Dr. William Goddard and Dr. Tahir Cagin for providing the CERIUS^2 applications. This work was supported by the United States−Israel Binational Science Foundation, the U.S. National Science Foundation, the Kimmelmann Center, the DanSync program of the Danish Natural Science Research Council, and the European Community under TMR-Contract ERBFMGECT950059. We thank HASYLAB for synchrotron beamtime.

JA002238T